ACS APPLIED MATERIALS & INTERFACES

Research Article

www.acsami.org

Understanding Interfacial Charge Transfer between Metallic PEDOT Counter Electrodes and a Cobalt Redox Shuttle in Dye-Sensitized Solar Cells

Byung-wook Park,[†] Meysam Pazoki,[†] Kerttu Aitola,[†] Seunghee Jeong,[‡] Erik M. J. Johansson,[†] Anders Hagfeldt,[†,§] and Gerrit Boschloo*[,†]

[†]Department of Chemistry, Ångström Laboratory, and [‡]Division of Solid-State Electronics, Ångström Laboratory, Uppsala University, Box 532, SE 751-20 Uppsala, Sweden

[§]School of Chemical Engineering, Sungkyankwan University, Suwon 440-746, Korea

Supporting Information

ABSTRACT: Conducting polymer poly(3,4-ethylenedioxythiophene) (PEDOT) doped with iron(III) tris-*p*-toluenesulfonate (PEDOT:Tos) having metallic conductivity was coated onto fluorine-doped tin oxide (FTO) glass and plain glass substrates and used as a counter electrode (CE) in a dye-sensitized solar cell (DSC) with a $[Co(bpy)_3]^{3+/2+}$ complex redox shuttle. DSCs with PEDOT:Tos/glass CE yielded power conversion efficiencies (PCE) of 6.3%, similar to that of DSCs with platinized FTO glass CE (6.1%). The PEDOT:Tos-based counter electrodes had 5 to 10 times lower charge-transfer resistance than the Pt/FTO CE in DSCs, as analyzed by impedance spectroscopy. More detailed studies in symmetrical CE-CE cells showed that the PEDOT:Tos layers are nanoporous. Not all internal area can be used catalytically under solar cell conditions and effective charge-transfer resistance was similar to that of Pt/FTO.

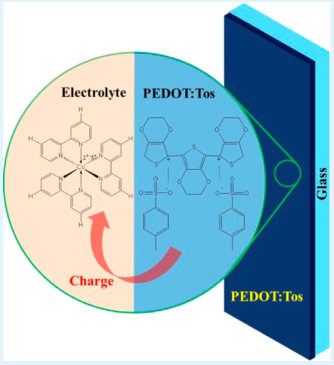

KEYWORDS: *dye-sensitized solar cells, counter electrode, electrocatalytic activity, metallic PEDOT, tosylate, Co complex electrolyte*

1. INTRODUCTION

Dye-sensitized solar cells (DSC) are attracting a lot of attention because of their high indoor power conversion efficiency and low cost compared to inorganic solar cells.[1−3] The DSC consists of a mesoporous TiO_2 film on a transparent conducting oxide-coated (TCO) glass substrate working electrode (WE), sensitized with dye molecules, a redox electrolyte, and a counter electrode (CE) composed of a platinum-coated TCO plate. Among these components, the TCO glass used both at the WE and the CE is a rather expensive component.[4] The most frequently used TCO in DSCs is fluorine-doped tin oxide (FTO). A relatively expensive component in the DSC is also the Pt catalyst at the counter electrode.

A number of investigations have been carried out to replace the Pt-coated FTO counter electrodes in DSCs by low-cost materials, such as different carbon species[5−11] and conducting polymers.[12−21] DSCs with carbon black-based counter electrodes have yielded record efficiencies of about 9% under 1 sun illumination.[11] With conducting polymers, micro-porous polyaniline CE for DSC resulted in a solar cells with a PCE of 7.1%.[13] DSCs with poly (3,4-propylenedioxythiophene) (PProDOT) coated onto FTO CE reached PCE of approximately 10%.[15] PEDOT-coated FTO CE in combination with a cobalt complex electrolyte have yielded a PCE of around 10%.[16]

Carli et al. compared the catalytic properties for PEDOT on FTO with ClO_4^-, sodium dodecylsulfate (SDS), or polystyrenesulfonate (PSS) as counterions to that of gold and platinum-coated FTO CE in cobalt complex-based electrolytes, where gold and PEDOT/ClO_4^- yielded the best results.[17] To further improve the counter electrode and the solar cell performance, researchers have investigated hybrid PEDOT counter electrodes, such as carbon nanotube/PEDOT, graphene/PEDOT, and metal/PEDOT.[18,19,27−29]

PEDOT is a promising alternative counter electrode material due to its high conductivity, electrochemical stability, semi-transparency, and catalytic performance. Because of its metal-like high conductivity, PEDOT:Tos can even replace TCO on the counter electrode to lower the cost of DSC fabrication.[4,18] Solar cell efficiencies of cells with Pt/TCO free counter electrode in combination with I^-/I_3^- redox mediator were comparatively good.

In this study, we employ a PEDOT:Tos coated CE with a cobalt(III/II) tris(2,2′-bipyridine) ($[Co(bpy)_3]^{3+/2+}$) complex-based redox mediator and compared it with the I^-/I_3^- redox mediator. The interfacial charge-transfer between the redox shuttles and the different CEs (Pt/FTO glass, PEDOT:Tos/

Received: November 16, 2013
Accepted: January 10, 2014
Published: January 10, 2014

   dx.doi.org/10.1021/am405108d | ACS Appl. Mater. Interfaces 2014, 6, 2074−2079

FTO glass and PEDOT:Tos/glass) are investigated using cyclic voltammetry and electrochemical impedance spectroscopy (EIS), and the performance of the CEs is analyzed in dye-sensitized solar cells.

2. EXPERIMENTAL SECTION

2.1. Preparation of PEDOT:Tos Counter Electrode. All chemicals were obtained from Sigma Aldrich and used as received. The oxidative polymerization of 3,4-ethylenedioxythiophene (EDOT) was carried out as follows. Iron(III) tris-*p*-toluenesulfonate hydroxide (iron tosylate/Fe(III) tosylate, 0.46 g, 8.08 mmol) was added in *n*-butanol (1.50 g, 1.53 mL) and filtered through a filter (Whatman, PVDF, 0.45 μm pore size). Pyridine was added as an inhibitor into the solution (0.046 g, 0.50 mmol per 1.00 mmol of tosylate) to control the kinetics of the polymerization. Finally, EDOT (0.051 g, 3.65 mmol) was added into the tosylate precursor and the solution was filtered. This precursor was spin-coated on glass and FTO glass (TEC15, Pilkington) substrates (typically 1.5 × 1.5 cm^2) at 1000 rpm. The use of tosylate is advantageous because it does not crystallize and, as a counter ion, it improves the film conductivity. After the coating, the films were dried and baked on a hot plate (5 min, 110 °C) under atmospheric condition. During the heating the EDOT polymerized. After cooling to room temperature, the films were washed several times in ethanol and acetonitrile to extract the iron(II) salts formed in the polymerization. The coating process was repeated for 20 times on the glass substrate and 8 times on the FTO glass substrate. The layer thickness was measured with a DEKTAK 3 profilometer. The thickness of the PEDOT:Tos layer on the FTO glass substrate and the glass substrate was about 420 and 1220 nm, respectively. The sheet resistances of the CE films were measured by four point probe and the results are displayed in Table S1 in the Supporting Information. Photographs of the different CEs are shown in Figure S2 in the Supporting Information.

2.1. Device Fabrication. The FTO glass plates were cleaned in subsequent order in detergent solution, water, 0.1 M HCl in ethanol, acetone, and EtOH using an ultrasonic bath for 30 min. The WE conducting glass substrates were then immersed in 40 mM aqueous $TiCl_4$ solution at 70 °C for 30 min and washed with water and ethanol. The 6 μm transparent nanocrystalline TiO_2 film was prepared by screen-printing Dyesol 18 NR-T paste diluted by 40 % in weight with 36 % terpineol and 4% ethyl cellulose on the FTO glass substrates. Scattering layer (4 μm) was also prepared by screen-printing using Dyesol WER2-O paste. The TiO_2 electrodes were gradually heated in an oven (Nabertherm Controller P330) in air. The temperature gradient program used four stationary plateaus at 180 °C (10 min), 325 °C (10 min), and 490 °C (30 min). After being cooled to around 90 °C, the electrodes were immersed in 0.25 mM organic dye (LEG4, see the SI Figure s-3) in ethanol and kept overnight in the dark at room temperature. After the dye-sensitization, the electrodes were rinsed with EtOH and dried in vacuum.

The Pt counter electrodes were prepared by applying 10 $\mu L/cm^2$ of 0.2 mM H_2PtCl_6 ethanolic solution on the FTO substrates and annealed at 400 °C for 30 minutes in an oven.

The WEs were sandwiched with the different counter electrodes using a 25 μm thick hot-melt film (Surlyn, Solaronix). The redox electrolyte was introduced through a hole drilled in the CE. Finally, the hole was sealed with the Surlyn film. The cobalt complex was purchased from Dyenamo AB (Sweden). The Co complex redox electrolyte consisted of 0.22 M $[Co(bpy)_3(PF_6)_2]^{2+}$, 0.05 M $[Co(bpy)_3(PF_6)_2]^{3+}$, 0.1 M $LiClO_4$, and 0.2 M 4-*tert*-butylpyridine in acetonitrile. The I^-/I_3^- electrolyte consisted of 0.03 M I_2, 0.6 M *n*-butyl-3-methylimidazolium iodide, 0.1 M guanidinium thiocyanate, 0.5 M 4-*tert*-butylpyridine in a mix of acetonitrile and valeronitrile (85:15 v/v). Silver paint was used to make contacts on the fabricated DSC.

2.2. Cyclic Voltammetry. Cyclic voltammograms of the Pt/FTO glass, PEDOT/FTO glass, and PEDOT/glass WEs were measured in a three electrode system. The counter electrode was a glassy carbon rod, the reference electrode was Ag/AgCl in acetonitrile, and the electrolyte was 2 mM $[Co(bpy)_3(PF_6)]^{2+}$ and 0.1 M $LiClO_4$ in acetonitrile. The voltage range was ±1.0 V or −1.0 to +1.5 at a scan rate of 50 mV s^{-1}, respectively. A potentiostat (Iviumstat, model EX) was used for measuring the CVs. A Teflon container was used for the measurement for each sample having the same surface area at the electrode/solution interface and the same distance between the working, counter, and reference electrodes in all the experiments.

2.3. Electrochemical Impedance Spectroscopy. The EIS measurements were carried out using an Autolab PGstat100 potentiostat equipped with an impedance module. The frequency range was from 10 kHz to 0.01 Hz and the amplitude of the AC perturbation 20 mV. The measurements were conducted under the dark condition at the open-circuit voltage. Zview2 program was used for fitting the data and the equivalent circuit contained the Bisquert model for the WE in SI Figure s-1.

2.4. Power Conversion Efficiency (PCE). The light source of a solar simulator for measuring the current−voltage (J−V) characteristics was a 300 W collimated xenon lamp (Newport) calibrated to a 1000 W m^{-2} light intensity at the 1.5 AM Global condition (1 sun AM 1.5 G illumination) by a certified silicon solar cell (Fraunhofer ISE). The electrical data were recorded with a computer controlled digital source-meter (Keithley Model 2400) with the scan direction from the open-circuit to the short-circuit at a scan rate of 50 mV s^{-1}. The DSC samples were masked during the measurement with an aperture area of 0.25 cm^2 (0.5 × 0.5 cm^2).

2.5. Incident Photon to Current Conversion Efficiency. The IPCE spectra were recorded with a computer-controlled setup comprised of a xenon lamp (Spectral Products, ASB-XE-175), a monochromator (Spectral Products, CM110), and a Keithley multimeter (Model 2700). The setup was calibrated with a certified silicon solar cell (Fraunhofer ISE) prior to the measurements. All DSCs were illuminated from the WE side with an aperture area of 0.2 cm^2 (0.4 × 0.5 cm^2) using a black mask.

3. RESULTS AND DISCUSSION

3.1. Photovoltaic Performance. Figure 1a represents the J−V characteristics of the devices with the three different CEs (Pt/FTO glass, PEDOT:Tos/FTO glass and PEDOT:Tos/glass). The light intensity-dependent photovoltaic parameters of the DSCs are summarized in Table 1. The solar cell efficiencies of the DSCs were of 6.1% (Pt/FTO), 6.5% (PEDOT:Tos/FTO), and 6.3% (PEDOT:Tos/glass). The fill factors (FF), current densities (J_{sc}), and open-circuit voltage (V_{oc}) are rather similar for all the DSCs under 1 sun illumination.

In the case of the I^-/I_3^- redox shuttle, however, significantly different tendencies of photovoltaic performances were found; see Figure S4 and Table S2 in the Supporting Information. DSCs with the PEDOT:Tos/glass CE displayed a very low photovoltaic performance, with a FF of 0.68, J_{sc} of 2.15 mA/cm^2, V_{oc} of 0.64 V, and PCE of 0.98 %. The PEDOT:Tos/FTO glass CE was significantly better with *FF* of 0.76, J_{sc} of 6.26 mA/cm^2, V_{oc} of 0.74 V and PCE 3.5 %. For comparison, the Pt/FTO glass CE was the best with a FF of 0.75, J_{sc} 7.84 mA/cm^2, V_{oc} 0.80 V and PCE 4.7 %.

According to Carli et al,[17] PEDOT:PSS coated CEs generally yield low fill factors in DSCs utilizing an I^-/I_3^- redox shuttle. The low electrocatalytic activity of the PEDOT:PSS towards the I^-/I_3^- redox shuttle has been explained by the reduced capability of forming charge-transfer adducts between the PEDOT holes and the I_3^- ion: the exposure of the negatively charged PSS-chains seems to prevent the approach of the I_3^- ion to the active sites of the PEDOT.[17] This limitation should not be important in the cationic Co complex redox shuttle, in which only the outer sphere electron-transfer events are involved and there seems to be no making or breaking of

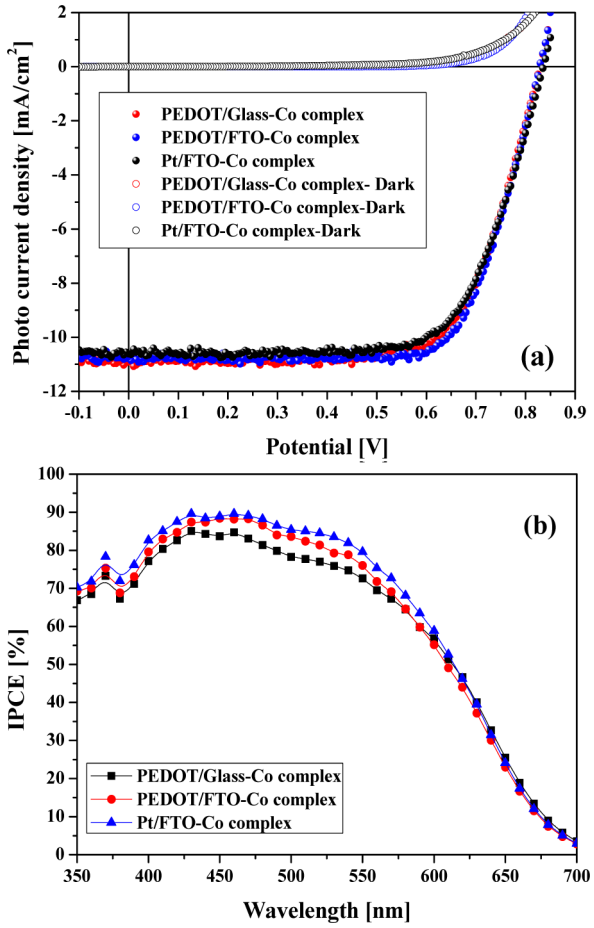

Figure 1. (a) Current density–voltage characteristics and (b) the IPCE spectra of the DSCs assembled using different CEs and a Co complex redox electrolyte.

chemical bonds unlike in the case of the I^-/I_3^- redox shuttle.[17,22,23]

3.2. Cyclic Voltammetry. Cyclic voltammetry was performed in order to check the catalytic activity of the prepared CEs and its relationship with the DSC photovoltaic performance. Figure 2 shows the cyclic voltammograms obtained from the Pt/FTO glass, PEDOT:Tos/FTO glass and PEDOT:Tos/glass CEs with the Co complex redox system. For all the CEs, a typical pair of oxidation/reduction peaks was clearly observed.[20,13]

The peak separation (E_{pp}) values of the CEs was 0.25 V (PEDOT:Tos/FTO glass), 0.47 V (PEDOT:Tos/glass) and 0.49 V (Pt/FTO glass). The smaller peak separation indicates higher electrocatalytic activities of the PEDOT:Tos/FTO glass and PEDOT:Tos/glass CEs as compared to that of the Pt/FTO glass CE. These results are in agreement with the larger charger-transfer resistance, R_{CT}, of the Pt/FTO glass CE as

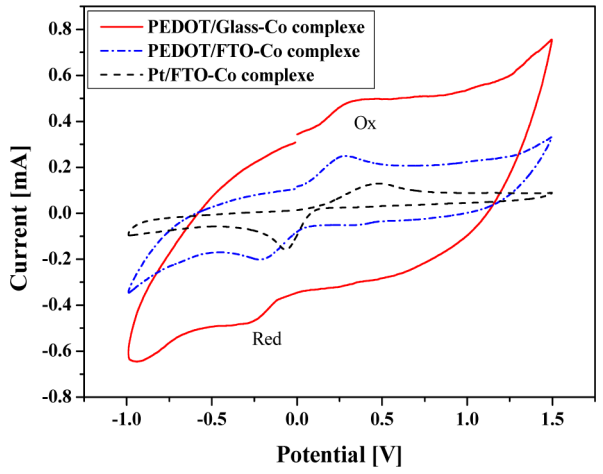

Figure 2. Cyclic voltammograms of the Pt/FTO glass, PEDOT:Tos/FTO glass, and PEDOT:Tos/glass CEs in cobalt electrolyte.

obtained from the EIS measurements, which will be discussed later (Table 2 and Figure 3).The PEDOT:Tos/FTO glass and

Table 2. DSC Series Resistance, the CE Charge-Transfer Resistance, and the CE Capacitance Values Obtained by the EIS Measurement of the DSCs

device type	R_S (Ω)	R_{CT} (Ω cm^2)	C_{CE} (F cm^{-2})
Pt/FTO	10.5	10.9	1.96×10^{-5}
PEDOT/FTO	13.4	2.7	6.86×10^{-6}
PEDOT/glass	15.2	1.1	1.90×10^{-4}

PEDOT:Tos/glass CEs display much higher background current densities than Pt/FTO CE, which is attributed to capacitive charging of the metallic PEDOT electrode. As the PEDOT:Tos/glass film is about three times thicker than the PEDOT:Tos/FTO glass, it appears that the PEDOT film is porous, so that the capacitive charging is proportional to the film thickness.

The cyclic voltammograms of the investigated counter electrodes with the I^-/I_3^- redox shuttle are shown in the SI Figure s-5. For all the CEs, two typical pairs of oxidation/reduction peaks (a and b) were clearly identified:[24–26]

$$I_3^- + 2e^- = 3I^- \quad \text{(a)}$$

$$3I_2 + 2e^- = 2I_3^- \quad \text{(b)}$$

The first pair of the redox peaks, the reduction of I_3^- to I^- (a) is important for the performance of CEs in DSC. The peak potential separation was larger for the PEDOT electrodes than for the Pt/FTO electrode.[26]

For both PEDOT:Tos electrodes, a third pair of redox peaks (c) could be seen. This pair may be attributed to the doping/dedoping of PEDOT, which is coupled to the movement of the

Table 1. *J–V* Characteristics of the DSCs at Various Light Intensities with the Cobalt Complex Electrolyte

	J_{sc} (mA/cm^2)			V_{oc} (mV)			FF			PCE (%)		
	light intensity (mW/cm^2)											
	100	46	11	100	46	11	100	46	11	100	46	11
Pt/FTO	10.6	5.7	1.4	0.84	0.82	0.78	0.69	0.74	0.70	6.1	7.4	6.9
PEDOT/FTO	10.7	5.6	1.4	0.83	0.81	0.77	0.73	0.77	0.78	6.5	7.6	7.4
PEDOT/glass	10.9	5.4	1.3	0.83	0.81	0.75	0.70	0.72	0.68	6.3	6.9	6.1

dx.doi.org/10.1021/am405108d | ACS Appl. Mater. Interfaces 2014, 6, 2074–2079

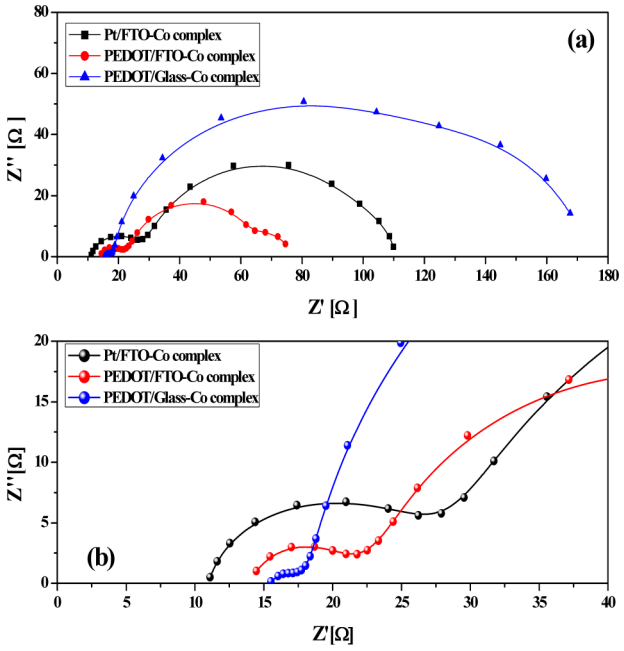

Figure 3. (a) Nyquist plots of the DSCs with Pt/FTO glass, PEDOT:Tos/FTO glass and PEDOT:Tos/glass. (b) Nyquist plots zoomed in the high-frequency area for better resolution of R_{CT}. Active area 0.49 cm^2.

inserted anions, as previously reported for the case of dodecyl sulfate in PEDOT.[13,20]

3.2. EIS Study of DSCs. Figure 3 shows the Nyquist plots of the EIS spectra for the DSCs with different CEs for the cobalt-based electrolyte (the region of higher-frequency is enlarged). In the high frequency region, the ohmic series resistance (R_S) and the charge-transfer resistance at the counter electrode (R_{CT}) can be determined based on the first semicircle (~kHz range). The second semicircle in the ~10−100 Hz range is related to the recombination resistance (R_{CR}) at the TiO_2/sensitizer/redox shuttle interface. The diffusion resistance of the redox shuttle is shown below ~10 Hz. The Bode plots of the spectra are displayed in Figure S4 in the Supporting Information. Table 2 shows the values for R_S, R_{CT}, and C_{CE} of the different CEs, obtained by the equivalent circuit fitting.

The DSCs show decreasing R_{CT} in order of Pt/FTO, PEDOT:Tos/FTO, and PEDOT:Tos/glass CEs in panels a and b in Figure 3 and Table 2. The series resistance is similar for all devices, demonstrating the excellent conductivity of PEDOT:Tos/glass. The R_{CT} of the Pt/FTO glass CE is rather high, 10.9 Ω cm^2, but low for the other CEs: 2.7 Ω cm^2 (PEDOT:Tos/FTO) and 1.1 Ω cm^2 (PEDOT:Tos/glass).

The increase of the C_{CE} could be related to the thicker PEDOT:Tos layer (greater nanoscopic surface area) on the glass substrate than the PEDOT:Tos layer on the FTO glass substrate. The larger nanoscopic surface area, as indicated by the larger C_{CE} of the PEDOT:Tos/glass than those of the other CEs, seems to be the reason for the lower R_{CT}. The trend differs from the results of a previous study by Ellis et al.,[27] in which a semiconducting PEDOT:sodium dodecylsulphate (PEDOT:SDS) film was studied as a DSC CE. In that study, the R_{CT} of the PEDOT:SDS CE was almost unaffected by the film thickness. Our results here, however, suggest that the R_{CT} decreases with the increasing PEDOT:Tos film thickness.

Impedance spectroscopy was also performed on solar cells with the I^-/I_3^- redox shuttle, see Figure S6 and Table S3 in the Supporting Information. In contrast to the cobalt electrolyte DSCs, the series resistance of the PEDOT:Tos/glass CE with the I^-/I_3^- redox shuttle is much higher than that of PEDOT:Tos/FTO and Pt/FTO CEs. The R_S value of the PEDOT:Tos/glass cells is related to the rather high sheet resistance of the PEDOT:Tos films after exposure to the electrolyte. The sheet resistances of the different CEs were measured by a four point probe before and after the measurement of the photovoltaic properties for DSCs and the results are summarized in Table S1 in the Supporting Information. It is apparent that the sheet resistance of PEDOT:Tos increases upon exposure to the redox electrolytes. The reason may be a certain de-doping of the PEDOT:Tos because of the redox electrolytes.

3.4. EIS Study of CE-CE Cells. To investigate the charge transfer at the PEDOT electrodes in more detail, we carried out EIS measurements on symmetrical CE-CE cells.[30,31] The impedance spectra taken at 0 V bias are presented in Figure 4. The equivalent circuit to analyze the data shown in Figure 4a and the Bode plots is shown in Figure S9 in the Supporting Information.

To fully understand PEDOT:Tos as a CE material, we have to consider its porous nature.[30,31] Specifically, an additional third semicircle appears in the Nyquist plot for the PEDOT counter electrodes that is attributed to porosity, see Figure 4b. The frequency response of the impedance of PEDOT:Tos CE is separated in two parts. According to Roy−Mayhew et al.,[30,31] the high frequency semicircle (100−2.5 kHz) can be attributed to a second Nernst diffusion impedance, resulting from the diffusion through the electrode pores in the PEDOT:Tos matrix (1:N_{PORE}) The middle semicircle (2500−25 Hz) represents the charge-transfer resistance and the capacitance of the catalytically active layer/electrolyte interface (2:R_{CT}, CPE). At very high frequencies, there are no diffusion limitations of the redox mediators in the nanopores of PEDOT, whereas at slower frequencies (and in DC) these limitations are apparent. Analyzing the high frequency part only would highly lead to a much too low value for the charge-transfer resistance. Finally, the low-frequency semicircle is ascribed to the bulk Nernst diffusion in the electrolyte (3:N_{BULK}), whereas the high-frequency offset determines the series resistance R_S. R_{CT} is an effective charge-transfer resistance, $R_{CT} = R_{CT} + N_{PORE}$. The values for the above-mentioned components obtained by the EIS spectra fitting for each CE-CE cell type are shown in Table 3.

In Table 3 and Figure 4, the R_S of the different CE-CE cells is shown to be 9.8 Ω (Pt/FTO glass CE), 17.3 Ω (PEDOT glass:Tos/FTO CE), and 237.0 Ω (PEDOT:Tos/glass CE). Those values are strongly related to the R_S resistances for each electrode. Particularly, the PEDOT:Tos-coated CEs have considerably higher values of R_S than each DSC CE, because the PEDOT:Tos layers of the CE-CE cell CEs were thinner than those of DSCs. However, we expect that it could not be influenced understanding the charge-transfer processes in these devices.

Figure 4a shows the two ordinary semicircles in the Nyquist plot of a cell consisting of two Pt/FTO glass CEs. The first semicircle and the second semicircle can be assigned to the R_{CT} and the N_{BULK}. Both had the value of about 1.9 Ω cm^2 (Table 3). The N_{PORE} does not appear. For the PEDOT/FTO glass CE-CE cells, three semicircles can be seen in Figure 4b. The

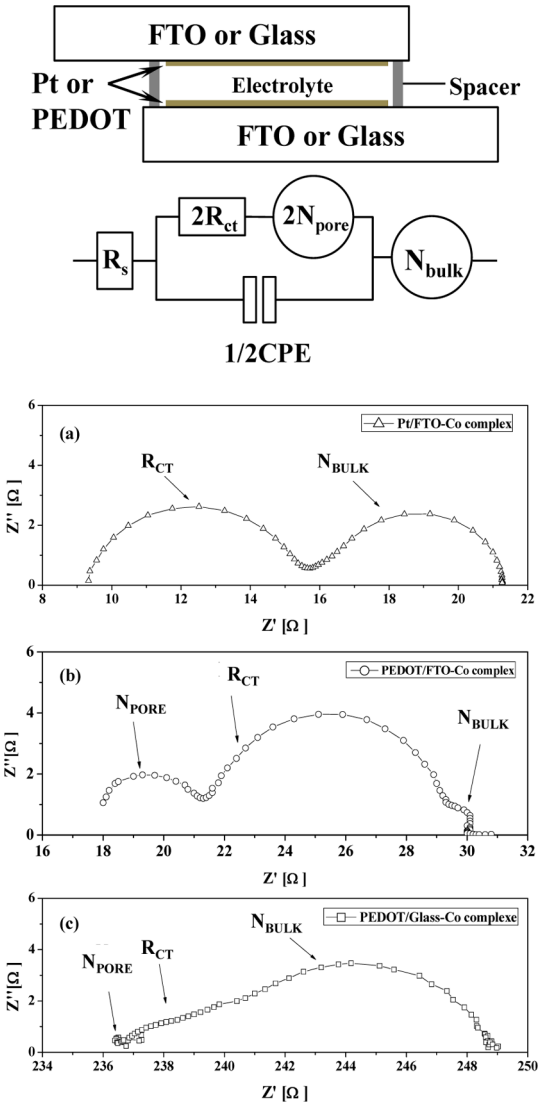

Figure 4. Nyquist plots for the different CE-CE cells. (a) Pt/FTO glass counter electrode, (b) PEDOT:Tos/FTO glass counter electrode (PEDOT film thickness about 220 nm), (c) PEDOT:Tos/glass counter electrode (PEDOT film thickness about 340 nm). Active area 0.64 cm^2.

Table 3. CE-CE Cell Series Resistance, CE Pore Diffusion Resistance, CE Charge-Transfer Resistance, Effective CE Charge-Transfer Resistance, and Bulk Diffusion Resistance Values Obtained by the EIS Measurement of the CE-CE Cells

CE-CE cell type	R_S (Ω)	N_{PORE} (Ω cm^2)	R_{CT} (Ω cm^2)	R_{CT} (Ω cm^2)	N_{BULK} (Ω cm^2)
Pt/FTO	9.3		1.9		1.9
PEDOT/FTO	17.3	1.0	2.0	3.0	0.5
PEDOT/glass	237.0	0.6	1.5	2.1	2.8

N_{PORE} value was 1.0 Ω cm^2, and R_{CT} and N_{BULK} were 2.0 and 0.5 Ω cm^2, respectively (Table 3). For the PEDOT:Tos/glass CE-CE cell, the three semicircles are not very clear in Figure 4c, but the Bode plot in FIgure S9c in the Supporting Information shows the frequencies for each elements of resistances and fitted values are 0.6 Ω cm^2 (N_{PORE}), 1.5 Ω cm^2 (R_{CT}), and 2.8 Ω cm^2 (N_{BULK}).

The overall charge-transfer resistance was similar for PEDOT:Tos/glass, PEDOT:Tos/FTO, and Pt/FTO.

Figure S8 in the Supporting Information show the Nyquist plots of the CE-CE cells with I^-/I_3^- redox shuttle. The values of R_S and N_{PORE} (see Table S4 in the Supporting Information) are similar as those of the CE-CE cells with the Co complex redox mediator. However, the overall charge-transfer resistance values for each CE are different for the two different electrolytes. The Pt/FTO value is about 3 times lower (0.7 Ω cm^2) than for the Co complex and the PEDOT:Tos/glass has around 2 times higher value (4.8 Ω cm^2).

4. CONCLUSION

In summary, counter electrodes for dye-sensitized solar cell based on PEDOT:Tos were fabricated by spin coating on glass and FTO glass substrates. The Pt- and TCO-free PEDOT:Tos/glass CE yielded solar cells with an efficiency of more than 6% for devices with cobalt-based redox electrolyte. This performance was similar to devices with Pt/TCO counter electrodes and PEDOT:Tos on FTO as counter electrode. The reason for the good photovoltaic performance was the good catalytic activity and the low charge-transfer resistance of the PEDOT:Tos electrodes in combination with cobalt bipyridine electrolytes. PEDOT:Tos electrodes performed less good in combination with I^-/I_3^- redox electrolytes. However, Pt- and FTO-free counter electrodes for dye-sensitized solar cells could be realized.

■ ASSOCIATED CONTENT

Ⓢ Supporting Information

Additional experiments on electrical equivalent circuit for EIS spectra of DSCs, images of counter electrodes, sheet resistances of each fabricated counter electrodes, a structure of a dye molecule, $J-V$ and IPCE curves, cyclic voltamogram of each fabricated counter electrodes for I^-/I_3^- redox shuttle, etc. This material is available free of charge via the Internet at http://pubs.acs.org.

■ AUTHOR INFORMATION

Corresponding Author

*E-mail: gerrit.boschloo@kemi.uu.se. Tel.: +46 184713303. Fax: +46 184713633.

Notes

The authors declare no competing financial interest.

■ ACKNOWLEDGMENTS

We thank the Swedish Energy Agency, the STandUP for Energy program, the Swedish Research Council (VR), the Göran Gustafsson Foundation, and the Knut and Alice Wallenberg Foundation.

■ REFERENCES

(1) Wang, P. S.; Zakeeruddin, M.; Comte, P.; Exnar, I.; Grätzel, M. *J. Am. Chem. Soc.* **2003**, *125*, 1166−1167.
(2) O'Regan, B.; Grätzel, M. *Nature* **1991**, *353*, 737−740.
(3) Hagfeldt, A.; Grätzel, M. *Acc. Chem. Res.* **2000**, *33*, 269−277.
(4) Lee, K. S.; Lee, H. K.; Wang, D. H.; Park, N. G.; Lee, J. Y.; Park, O O.; Park, J. H. *Chem. Commun.* **2010**, *46*, 4505−4507.
(5) Ramasamy, E.; Lee, J. *Chem. Commun.* **2010**, *46*, 2136−2138.
(6) Kay, K.; Grätzel, M. *Sol. Energy Mater. Sol. Cells* **1996**, *44*, 99−117.

(7) Papageorgiou, N.; Liska, P.; Kay, A.; Gratzel, M. *J. Electrochem. Soc.* **1999**, *146*, 898−907.
(8) Papageorgiou, N.; Moser, W. F.; Gratzel, M. *J. Electrochem. Soc.* **1997**, *144*, 876−884.
(9) Suzuki, K.; Yamaguchi, M.; Kumagai, M.; Yanagida, S. *Chem. Lett.* **2003**, *32*, 28−29.
(10) Imoto, K.; Takahashi, K.; Yamaguchi, T.; Komura, T.; Nakamura, J.; Murata, K. *Sol. Energy Mater. Sol. Cells* **2003**, *79*, 459−469.
(11) Murakami, T. N.; Ito, S.; Wang, Q.; Nazeeruddin, M. K.; Bessho, T.; Cesar, I.; Liska, P.; Humphry-Baker, R.; Comte, P.; Pechy, P.; Gratzel, M. *J. Electrochem. Soc.* **2006**, *153*, A2255−A2261.
(12) Lee, K. M.; Chen, P. Y.; Hsu, C. Y.; Huang, H. H.; Ho, W. H.; Chen, H. C.; Ho, K. C. *J. Power Sources* **2009**, *188*, 313−318.
(13) Li, Q.; Wu, J.; Tang, Q.; Lan, Z.; Li, P.; Lin, J.; Fan, L. *Electrochem. Commun.* **2008**, *10*, 1299−1302.
(14) Ahmad, S.; Yum, J. H.; Xianxi, Z.; Gratzel, M.; Butt, H. J.; Nazeeruddin, M. K. *J. Mater. Chem.* **2010**, *20*, 1654−1658.
(15) Yum, J.-H.; Baranoff, E.; Kessler, F.; Moehl, T.; Ahmad, S.; Bessho, T.; Marchioro, A.; Ghadiri, E.; Moser, J.-E.; Yi, C.; Nazeeruddin, Md. K.; Grätzel, M. *Nat. Commun.* **2012**, *631*, DOI: 10.1038/ncomms1655.
(16) Tsao, H. N.; Burschka, J.; Yi, C.; Kessler, F.; Nazeeruddin, M. K.; Grätzel, M. *Energy Environ. Sci.* **2011**, *4*, 4921−4924.
(17) Carli, S.; Busatto, E.; Caramori, S.; Boaretto, R.; Argazzi, R.; Timpson, C. J.; Bignozzi, C. A. *J. Phys. Chem. C* **2013**, *117*, 5142−5153.
(18) Lee, K. S.; Lee, Y.; Lee, J. Y.; Ahn, J.-H.; Park, J. H. *ChemSusChem* **2012**, *5*, 379−382.
(19) Lee, K. S.; Yun, J. H.; Han, Y.-H.; Yim, J.-H.; Park, N.-G.; Cho, K. Y.; Park, J. H.; Mater., J. *Chem. Commun.* **2011**, *21*, 15193−15196, DOI: 10.1039/c1jm13408f.
(20) Lee, T. H.; Do, K.; Lee, Y. W.; Jeon, S. S.; Kim, C.; Ko, J.; Im, S. S. *J. Mater. Chem.* **2012**, *22*, 21624−21629.
(21) Xia, J. B.; Masaki, N.; Jiang, K. J.; Yanagida, S. *J. Mater. Chem.* **2007**, *17*, 2845−2850.
(22) Saito, Y.; Kitamura, T.; Wulia, Y.; Yanagida, S. *Chem. Lett.* **2002**, 1060−1061.
(23) Saito, Y.; Kubo, W.; Kitamura, T.; Wada, Y.; Yanagida, S. *J. Photochem. Photobiol., A* **2004**, *164*, 153−157.
(24) Popov, A. I.; Geske, D. H. *J. Am. Chem. Soc.* **1958**, *80*, 1340−1352.
(25) Sakurai, S.; Jiang, H. Q.; Takahashi, M.; Kobayashi, K. *Electrochim. Acta* **2009**, *54*, 5463−5469.
(26) Jeon, S. S.; Kim, C.; Ko, J.; Im, S. S *J. Phys. Chem. C* **2011**, *115*, 22035−22039.
(27) Ellis, H.; Vlachopoulos, N.; Häggman, L.; Perruchot, C.; Jouini, M.; Boschloo, G.; Hagfeldt, A. *Electrochimica Acta* **2013**, *107*, 45−51.
(28) Liberatore, M.; Petrocco, A.; Caprioli, F.; La Mesa, C.; Decker, F.; Bignozzi, C. A. *Electrochim. Acta* **2010**, *55*, 4025−4029.
(29) Cameron, P. J.; Peter, L. M.; Zakeeruddin, S. M.; Graetzel, M. *Coord. Chem. Rev.* **2004**, *248*, 1447−1453.
(30) Roy-Mayhew, J. D.; Bozym, D. J.; Punckt, C.; Aksay, I. A. *ACS Nano* **2010**, *4* (10), 6203−6211.
(31) Roy-Mayhew, J. D.; Boschloo, G.; Hagfeldt, A.; Aksay, I. A. *ACS Appl. Mater. Interfaces* **2012**, *4*, 2794−2800.